Controlling mid-infrared plasmons in graphene nanostructures through post-fabrication chemical doping

Journal of Physics: Photonics

OPEN ACCESS

RECEIVED
30 December 2020

REVISED
25 March 2021

ACCEPTED FOR PUBLICATION
19 April 2021

PUBLISHED
7 May 2021

PAPER

Controlling mid-infrared plasmons in graphene nanostructures through post-fabrication chemical doping

Bruno Paulillo[1,*], **Nestor Jr Bareza**[1] and **Valerio Pruneri**[1,2]

[1] ICFO-Institut de Ciencies Fotoniques, The Barcelona Institute of Science and Technology, 08860 Castelldefels, Barcelona, Spain
[2] ICREA-Institució Catalana de Recerca i Estudis Avançats, Passeig Lluís Companys, 23, 08010 Barcelona, Spain
[*] Author to whom any correspondence should be addressed.

E-mail: bruno.paulillo@icfo.eu

Keywords: graphene plasmonics, chemical doping, mid-infrared, graphene sensors

Supplementary material for this article is available online

Abstract

Engineering the doping level in graphene nanostructures to yield controlled and intense localized surface plasmon resonance (LSPR) is fundamental for their practical use in applications such as molecular sensing for point of care or environmental monitoring. In this work, we experimentally study how chemical doping of graphene nanostructures using ethylene amines affects their mid-infrared plasmonic response following the induced change in electrical transport properties. Combining post-fabrication silanization and amine doping allows to prepare the surface to support a strong LSPR response at zero bias. These findings pave the way to design highly doped graphene LSPR surfaces for infrared sensors operating in real environments.

1. Introduction

Graphene has attracted a huge interest as electronic, optical and optoelectronic material due to its extraordinary properties including optical transparency, tunable ambipolar electrical conductivity and high carrier mobility [1, 2]. Graphene-based technology has evolved at fast pace in recent years strongly impacting several fields, including transparent electronics [3] and thin-film transistor sensors [4, 5]. Simultaneously, nanostructured graphene surfaces have emerged as a unique platform for IR nano-optics since graphene tunable conductivity results into a reconfigurable plasmonic response at mid-infrared (mid-IR) wavelengths [6, 7]. Reported applications of graphene plasmonics include IR photodetection, enhanced light–matter interaction and molecular gas or bio sensing [8–10]. For instance, graphene nano-ribbons (GNRs) [11] or nano-holes [12] exhibit extremely confined localized surface plasmon resonances (LSPRs) that can be spectrally and intensity tuned by changing the graphene Fermi level via electrostatic or chemical surface doping. The highly subwavelength field decay of graphene LSPR (<15 nm) allows sensing of tiny molecules (∼nm) through their mid-IR vibrational fingerprints or interaction with specific functional layers that modify graphene electro-optical response [8]. Several recent studies have highlighted the tremendous application potential of graphene LSPR for sensors based on surface enhanced infrared absorption (SEIRA) [13, 14]. However, in these proof-of-concept experiments a full comparison between electrical and plasmonic properties was not given and the role of fabrication process influencing the initial doping level of graphene nanostructures was mostly neglected. While it is easy to dynamically set the Fermi level *a posteriori* through capacitive or electrochemical gating, for many applications it is desirable to engineer and stabilize graphene doping in a back-end process, prior to device operation. In fact, manipulating the initial doping level of graphene nanostructures is fundamental to move from lab experiments to marketable graphene plasmonic sensors where robust and reproducible LSPR excitations are required.

In this paper, we propose a simple method to control the doping level of graphene plasmonic surfaces using post-fabrication silanization and chemical doping based on ethylene amines. We report a detailed experimental study of graphene nanostructures prepared with conventional nanofabrication methods and subsequently treated with amine-containing chemicals highlighting the relation between electrical properties

and mid-infrared optical response. We conclude discussing potential applications of this work to novel LSPR sensing platforms based on chemically doped graphene.

2. Experimental section

2.1. Graphene nanostructures fabrication

Graphene field effect transistors (GFETs) were fabricated using a two-step photolithography process on a double polished silicon substrate with a top thermally grown 300 nm thick SiO_2 layer. First, Ti/Au (3/40 nm) contacts were defined via lift-off using a positive tone photoresist (S1805). Graphene grown by chemical vapour deposition (from Graphenea Inc.) was then wet-transferred on the metallized substrate. GFETs channel regions were patterned using a negative tone photoresist (AZ nLOF2020) and reactive ion etching in an oxygen/argon plasma. The Au/Graphene contact area for each electrode is 0.2×1 mm^2.

Arrays of GNRs of different dimensions were defined in the GFET channel using a spin-coated 40 nm thick electron beam resist (ZEP520A) and a 50 keV electron beam lithography system. After development, the exposed graphene regions were etched in an oxygen/argon plasma. The residual resist was then stripped off using N-Methyl-2-pyrrolidone (NMP).

2.2. Chemical doping protocols

As-prepared GFETs and graphene nanostructures were treated by hexamethyldisilazane (HMDS, from Merck) before chemical doping following the protocols used in [15, 16]. The chips were immersed in a HMDS/acetone (1/1) bath under a fume hood for 12–15 h.

For graphene vapour doping, a protocol similar to what reported in [17] was used. Tetraethylenepentamine (TEPA, from Merck) was the graphene dopant. Each chip was placed in a Petri dish next to a piece of cleanroom wiper where a few droplets (approx. 60 μl) of TEPA were dropped. The closed Petri dish was placed on a hotplate and baked at 95 °C for 30 min.

For graphene polymer doping, a 0.2 wt% solution of branched polyethylenimine (PEI, Mw $\sim$ 25000 from Merck) in ethanol was prepared using a magnetic stirrer. The PEI solution was spin-coated on the chip at 5000 rpm and the chip was baked at 100 °C for 2 min.

2.3. Electrical characterization

The two-point resistance R of GFETs channel as a function of the applied back-gate voltage V_{BG} was monitored in a probe station equipped with two precision source-meter units (Keysight B2901). The R–V_{BG} curves were recorded several times for each device to confirm reproducibility of the measurement response and hysteresis cycle. Note that the reported two-point R values have the same magnitude of typical graphene sheet resistance (R_s) values since the graphene channel is square-shaped. However, for a precise measurement of R_s values, the data should be corrected to include the contact resistance contribution [18].

2.4. Optical characterization

A FTIR spectrometer (Bruker Tensor II) equipped with an IR microscope (Bruker Hyperion 2000) and a nitrogen-cooled MCT detector was used to collect the transmission spectra of graphene nanostructures. A reflective objective with NA = 0.4 and 15× magnification was used to focus the beam onto the chip surface. IR light was polarized perpendicular to the nano-ribbons orientation. Subsequent measurements were taken on regions with GNRs (signal, T) and without them (background, T_0). Extinction is defined as $1 - T/T_0$.

3. Results and discussion

Figure 1(a) shows a sketch of the GFET structure used in this work. The channel is a graphene square of 1 mm^2 area connected to Ti/Au contact pads (contact area Au/graphene is 0.1×1 mm^2). The Si/SiO_2 substrate allows to modulate the channel conductivity by applying a voltage V_{BG} to the back Si surface. The channel resistance as a function of V_{BG} can be read between the two graphene contacts. A picture of a fabricated GFET is reported in figure 1(b). The typical electrical behaviour of such GFET structure after fabrication ('as-prepared') is shown in the top panel (green curve) of figure 1(c). We note that the V-shaped Dirac curve starts to appear in the right part corresponding to positive V_{BG}, and the charge neutrality point (CNP) voltage V_{CNP} is located beyond +100 V. By definition $V_{CNP} > 0$ means that the as-prepared GFET is initially p-doped, and the majority carriers are holes. This is common for GFETs fabricated with standard lithographic processes, typically yielding $0 < V_{CNP} < +100$ V [19, 20]. Here the fact that a cross-linked negative photoresist is used to define the GFET channel could explain the higher p-doping [21]. In addition, the Dirac curve shows hysteresis when changing the voltage sweep direction that is associated to process-related defects, polymer residues and/or water molecules adsorbed on graphene or substrate [19].

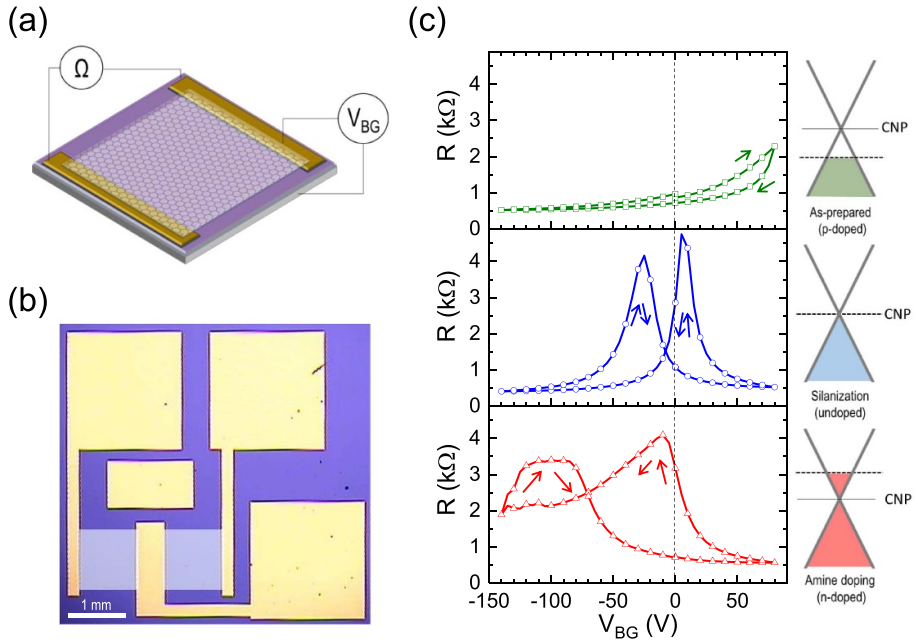

Figure 1. (a) Conceptual view and (b) real picture of the GFET structure used in this work. The graphene area for each GFET is 1 mm^2. (c) Measured resistance (R) versus back-gate voltage (V_{BG}) curves for as-prepared (top), HMDS-treated (middle) and TEPA-vapour doped (bottom) GFET structure. A sketch of the Dirac cone and doping level for each doping process is shown on the right side.

To revert the fabrication-related GFET doping silanization with HMDS surface treatment or vacuum annealing have been proposed [15, 16, 20]. In particular, treating the devices after fabrication with HMDS constitutes an easy way to reduce substantially the initial p-doping regardless the specific fabrication protocol (e.g. resist used). In the central panel (blue curve) of figure 1(c) we report the R–V_{BG} curve for the same GFET device after HMDS treatment. We observe that the CNP voltage is substantially lowered and approaches 0 V meaning that the graphene is brought close to its pristine state. This is advantageous since it allows to bring back the GFET to a controlled initial CNP, prior to any subsequent process to reach the target doping. For this structure a relatively large hysteresis in the R–V_{BG} curve remains after HMDS treatment ($V_{CNP} = +5$ V when sweeping from positive to negative and $V_{CNP} = -25$ V when sweeping from negative to positive), unlike what expected from HMDS treatment [15, 16].

Next, we employ a simple vapour-phase molecular doping process with a high-molecular-weight ethylene amine (TEPA) to modify the GFET electrical behaviour, as shown in the bottom panel (red curve) of figure 1(c). TEPA and other ethylene amines have been studied in detail as strong n-dopants for graphene devices with ease of process and acceptable stability over time for practical applications [17, 22]. The Dirac curve after TEPA doping shows a highly hysteretic behaviour with $V_{CNP} = -120$ V when sweeping from negative to positive bias and V_{CNP} close to 0 V when sweeping from positive to negative bias. In the first case, the CNP position induced by chemical doping is consistent with literature and corresponds to a strongly n-doped GFET where the electrical conduction is dominated by free electrons (right side of Dirac curve) in the useful V_{BG} range (typically $|V_{BG}| \leqslant 150$ V to avoid SiO_2 breakdown). Conversely, in the latter case the Dirac curve is almost centred but highly asymmetric with respect to the CNP. A similar asymmetry was reported for other GFETs doped with amines (e.g. PEI) and is related to a partial suppression of the free holes conduction [23], an effect also observed for ambipolar organic semiconductors [24]. The R–V_{BG} curve was measured for several devices after both the HMDS treatment and TEPA vapor doping process showing good reproducibility (see figure S2 in SI (available online at stacks.iop.org/JPPHOTON/3/034001/mmedia)). The results are in agreement with published data [16, 17] with a small chip-to-chip variation that can be explained in terms of differences of process conditions. Also, the modification of Raman spectra (see figure S1 in SI) and, specifically, the reduction of the I_{2D}/I_G ratio after vapor doping is similar to previous literature reports [17].

Let us now consider how the chemical doping described above affects the optical behaviour of graphene, especially at IR wavelengths where its plasmonic response is tightly related to free carriers motion.

To investigate the amine doping effect on IR graphene plasmons, we nano-patterned the graphene channel of a GFET structure to excite a mid-IR LSPR mode [11, 13] (see figure S5 in SI for LSPR

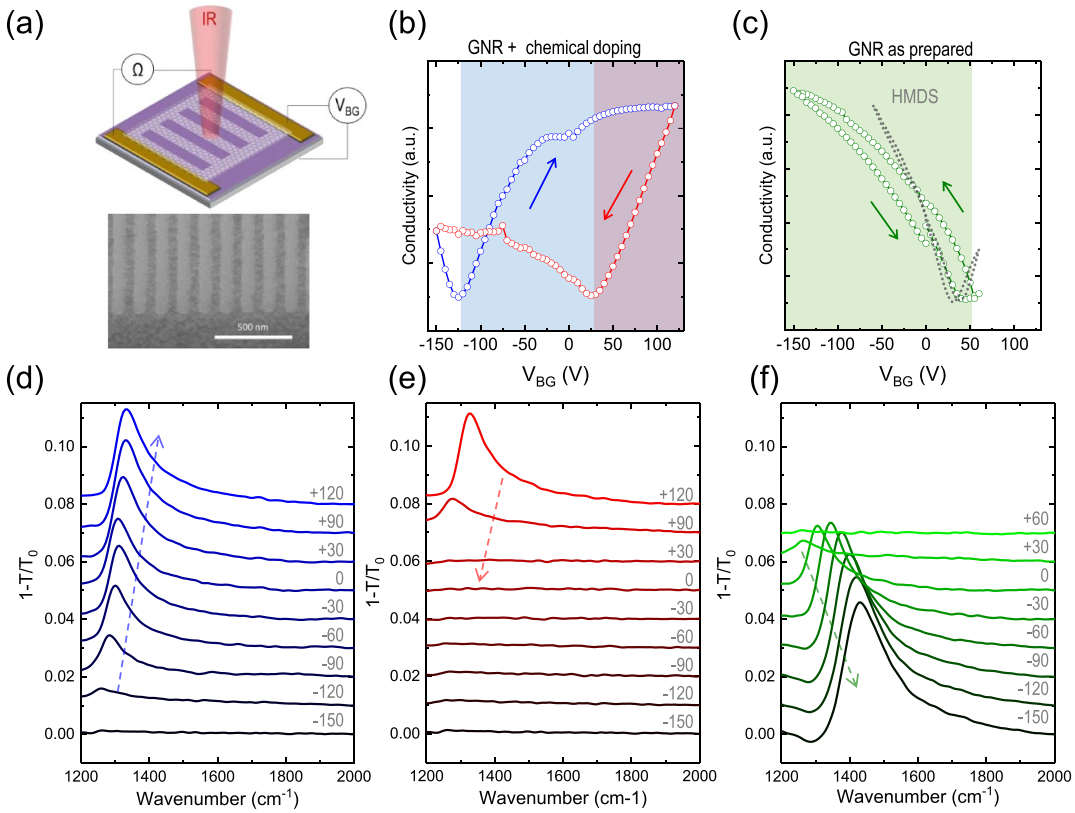

Figure 2. (a) Conceptual view of the GFET structure with nano-patterned graphene. The SEM picture shows the EBL-patterned GNR array. (b) σ_{2D} vs V_{BG} curve for the HMDS + TEPA treated GNR-GFET for negative to positive (blue) and positive to negative (red) sweep. (c) σ_{2D} vs V_{BG} curve for the as prepared (green) and HMDS treated (grey) GNR-GFET. (d) IR extinction spectra for TEPA-doped GNR array for V_{BG} sweep from negative to positive bias. (e) IR extinction spectra for TEPA-doped GNR array for V_{BG} sweep from positive to negative bias. (f) IR extinction spectra for as-prepared GNR array for V_{BG} sweep from positive to negative bias. Dashed arrows indicate LSPR growth. Spectra are vertically stacked for clarity.

characterization). In such a device, we can both assess the electrical response and the optical spectrum upon V_{BG} by FTIR microscopy. A conceptual view of the experiment is shown in figure 2(a). We use a standard graphene GNR geometry (SEM of bottom panel of figure 2(a)), with ribbon width $w = 70$ nm and array period $p = 140$ nm to have a plasmonic resonance around $\lambda = 7$ μm. After patterning, the GFET + GNR device underwent HMDS treatment and TEPA vapor doping. In figure 2(b) we report the surface electrical conductivity $\sigma_{2D} \propto 1/R$ versus applied V_{BG} where R is the electrical resistance between the two Au contacts. Note that the curve represents a full V_{BG} cycle acquired continuously (as in figure 1(c)) but we plotted the two branches with different colours to distinguish the dependence on sweep direction. We observe that the response is similar to the one in the bottom panel of figure 1(c) with $V_{CNP} = -125$ V induced by chemical doping when sweeping from negative to positive bias. The shadowed areas in the graph represent the regions where plasmon modes are visible for each sweep direction (see below).

For comparison, in figure 2(c) the electrical response for the as-prepared GFET + GNR structure (green curve) and the structure after HMDS treatment (grey curve) are shown. Note that the initial surface doping of the GFET + GNR structure ($V_{CNP} \approx +50$ V) differs from the bare GFET structure due to the additional EBL step and is consistent with the typical reported response of GNRs prepared by EBL [25, 26]. Furthermore, the CNP position is slightly lowered by the HMDS treatment and the curve hysteresis is noticeably reduced, as observed in other reports [15, 16].

Let us discuss now how the electrical behaviour affects the excitation of plasmon modes upon gating. In figure 2(d) the IR extinction spectrum of the TEPA-doped GNR surface is shown for V_{BG} sweeping from negative (-150 V) to positive ($+120$ V) voltage. The LSPR resonance appears at $V_{BG} = -120$ V and gradually blue-shifts and grows in intensity as V_{BG} is increased. Conversely, when going from positive to negative V_{BG} the LSPR resonance quickly fades out and is not visible when crossing zero voltage (figure 2(e)). As expected, the LSPR excitation follows the σ_{2D}–V_{BG} curve since graphene plasmon dispersion is related to the free carrier optical conductivity [27]. Interestingly, the LSPR mode appears only

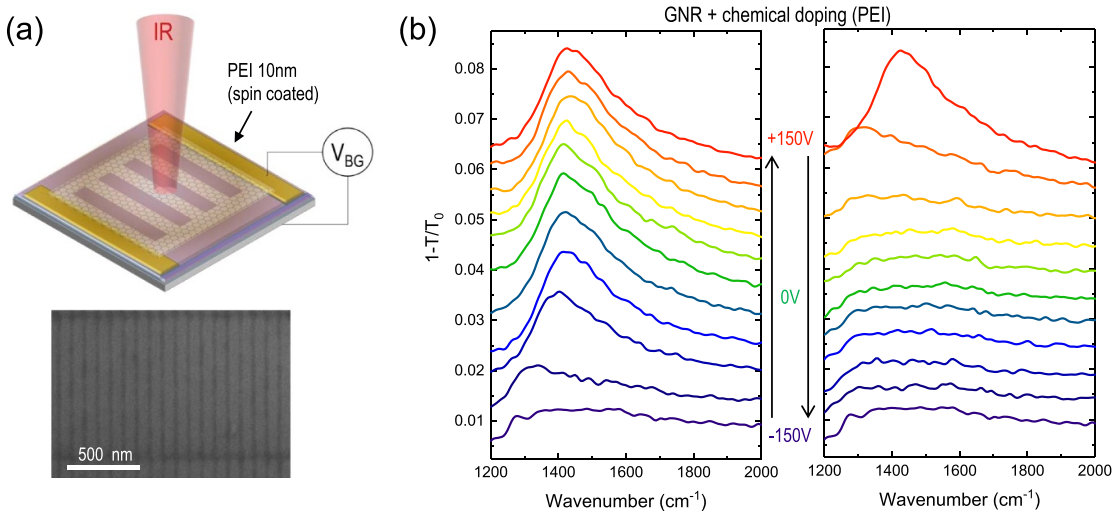

Figure 3. (a) Conceptual view of the GFET structure with nano-patterned graphene and PEI coating. The SEM picture shows the EBL-patterned GNR array probed in the optical characterization. (b) IR extinction spectra for PEI-doped GNR array for V_{BG} sweep from negative to positive (left) and positive to negative (right) bias.

when $V_{BG} > V_{CNP}$ i.e. when the graphene is filled with electrons (right side of the Dirac curve), while the increase of conductivity for $V_{BG} < V_{CNP}$ (left side of the Dirac curve) does not produce any plasmon excitation. This could be due to the fact that adsorbed amine molecules act as long range scatterers for holes in graphene [23], damping charge oscillations that originate plasmons. For comparison, figure 2(f) reports the plasmonic response of the as-prepared GNR surface before HMDS treatment and TEPA doping. The LSPR mode blue-shifts and grows for increased negative voltages, in agreement with the electrical response curve and previous literature reports.

These results show that chemical doping based on amine molecules can be used to prepare GNRs with a defined Fermi level that translates into a strong LSPR response, notably at $V_{BG} = 0$ V. We also highlight that, even for as-prepared GNRs, the electrical hysteresis plays a non-negligible role in the observed doping level at a fixed V_{BG}. This has to be considered when using these surfaces for e.g. quantitative molecular sensing, where a quantification of the analyte-induced LSPR spectral shift or intensity is needed [13, 25].

Next, we show that a similar plasmonic response is obtained when graphene nanostructures are coated with an ultra-thin, amine-containing polymer such as polyethylenimine (PEI). PEI thin films have been recently used as selective functional adsorbers for surface-enhanced IR gas sensing due to their chemical selectivity against CO_2 and VOCs molecules [28]. Furthermore, a new LSPR sensing scheme based on the reversible chemical doping effect of PEI on graphene upon gas adsorption was proposed [25]. However, spin-coated PEI has been shown to yield a lower doping level than vaporized high molecular weights amines (e.g. TEPA) [17]. In figure 3(a) a sketch of a GNR surface coated with an ultra-thin PEI layer is shown. The IR optical response under a full cycle of V_{BG} is reported in figure 3(b). Both the left panel (V_{BG} sweep from -150 V to $+150$ V) and right panel (V_{BG} sweep from $+150$ V to -150 V) show a trend similar to figures 2(d)–(e). Again, note that the doping state at 0 V (green curves) changes depending on the sweep direction and, when starting at $V_{BG} < 0$, a strong LSPR mode is visible at zero bias.

Long-term stability of chemical doping is a key aspect for practical applications. The n-doping effect from different vaporized amine molecules was shown to be slightly reduced after several (≈20) days of storage in air [22]. In our case, for TEPA doping we observed a similar behaviour with a reduction of the CNP voltage of $\Delta V_{CNP} \approx 25$ V after 2 weeks of storage in air (see figure S4(a) in SI). This is possibly due to the fact that the adsorbed molecular layer tends to be slowly desorbed from the surface yielding a reduction of the n-doping effect. However, a very high conductivity is still observed at zero bias. On the other hand, ultra-thin PEI layers show a stable doping effect after 20 days of operation [25], albeit weaker than what obtained with vaporized high-molecular weights amines [17]. In SI-figure S4(b) we propose the combination of TEPA doping and ultra-thin PEI as capping layer to obtain a strong n-doping effect which is sufficiently stable over time.

In the next section we discuss how these results can pave the way to obtain highly doped graphene SEIRA surfaces using GNRs.

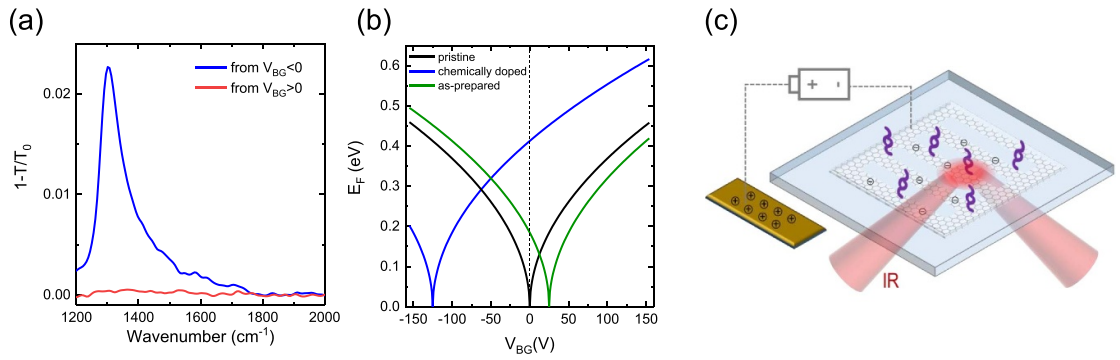

Figure 4. (a) Extinction spectra for the GNR–GFET surface disconnected from voltage source after sweeping from negative (blue) and positive V_{BG} (red) to zero bias. (b) Calculated Fermi level (E_F) as a function of the CNP position for pristine, as-prepared and chemically doped graphene. (c) Conceptual view of a chemically-doped LSPR surface on transparent IR substrate for molecular sensing.

4. Application

In figure 4(a) we show the extinction spectrum of the GFET–GNR sample of figure 2 at zero bias after disconnecting the gate voltage source. We observe a strong LSPR response when sweeping to zero from negative bias (blue curve) while no plasmonic response is visible when coming from positive bias (red curve). This suggests that one can prepare the chemically-doped GNR surface to stay in a high conductivity state (i.e. high Fermi level) at zero bias by properly 'charging' the graphene surface. In figure 4(b) we calculate the equivalent Fermi level (in eV) for different CNP voltages corresponding to pristine graphene (black), as-prepared GNR (green) and chemically doped GNR (blue) studied in this work using the formula reported in [29]. Note that using high molecular-weight amines at zero bias a Fermi level $E_F \geqslant 0.4$ eV is reached, similar to the maximum doping level that could be achieved via Si/SiO_2 back-gating at high voltage ($V_{BG} \leq -100$ V).

These findings, while preliminary, are relevant for applications where a bright LSPR mode is needed such as GNR surfaces for SEIRA molecular sensing. On the one hand, the GNRs could be operated at zero bias, with no need to apply a high gate voltage like in conventional counterparts on Si/SiO_2. On the other hand, one would be free from any constraints imposed by the conventional Si/SiO_2 substrate (e.g. opacity at NIR/VIS wavelength) and/or gate geometry. After chemical doping, the surface could be prepared in the desired conductivity state through low-cost electrolyte gating and then functionalized with a layer of relevant recognition elements. In particular, amine-based protocols are emerging to functionalize graphene with relevant biomarkers such as DNA strands or aptamers [30, 31]. This could lead to novel bio-sensing schemes where LSPR is tuned upon interaction of biomolecules with aminated GNRs similarly to what recently shown in gas sensing experiments [25].

As an example, in figure 4(c) we sketch a graphene LSPR sensing surface built on an IR transparent substrate (e.g. CaF_2). Due to the high surface transparency and absence of a back-gate structure, the chip could be used in a variety of optical configurations, including operation in water ambient with back-reflection readout as in commercial SPR devices.

Finally, the combination of graphene chemical doping, large-scale nanopatterning [32] and emerging IR substrates (e.g. ceramics, plastic) [33, 34] could lead to a new generation of graphene-based LSPR optical sensors that are mechanically flexible, broadly transparent, mass-scalable and potentially low-cost.

5. Conclusions

In conclusion, we fabricated GFET structures with nano-patterned channel region to study the optical behaviour of mid-IR graphene LSPR modes upon post-fabrication chemical doping. We reported a complete step by step electrical and optical charcterization to highlight how the plasmonic response follows the change in electrical transport induced by the n-type doping process. We found a similar behavior when reversing the gate sweep direction for ethylene amines vapour (TEPA) or polymer (PEI) doping. Potential applications of this study include the design of highly doped graphene LSPR surfaces on non-conventional substrates for bio and gas molecular sensing in relevant environment.

Data availability statement

The data that support the findings of this study are available upon reasonable request from the authors.

Acknowledgments

The research leading to these results has received funding from the H2020 Programme under Grant Agreement No. 881603 (Graphene Flagship). This project has received funding from the European Union's Horizon 2020 research and innovation programme under the Marie Skłodowska-Curie Grant Agreement No. 754510. This project has received funding from the European Union's Horizon 2020 research and innovation programme under the Marie Skłodowska-Curie Grant Agreement No. 665884. We acknowledge financial support from the Spanish Ministry of Economy and Competitiveness through the 'Severo Ochoa' Programme for Centres of Excellence in R&D (CEX2019-000910-S) and project TUNA-SURF (PID2019-106892RB-I00), Fundació Mir-Puig, and from Generalitat de Catalunya through the CERCA program, from AGAUR 2017 SGR 1634.

We thank Christina Graham for help with Raman characterization.

ORCID iDs

Bruno Paulillo https://orcid.org/0000-0002-6675-0141
Nestor Jr Bareza https://orcid.org/0000-0002-0562-650X

References

[1] Grigorenko A N, Polini M and Novoselov K S 2012 *Nat. Photon.* **6** 749
[2] Castro Neto A H, Guinea F, Peres N M R, Novoselov K S and Geim A K 2009 *Rev. Mod. Phys.* **81** 109
[3] Mustonen P, Mackenzie D M A and Lipsanen H 2020 *Front. Optoelectron.* **13** 91
[4] Fu W, Jiang L, Van Geest E P, Lima L M C and Schneider G F 2017 *Adv. Mater.* **29** 1603610
[5] Zhan B, Li C, Yang J, Jenkins G, Huang W and Dong X 2014 *Small* **10** 4042
[6] Brar V W, Jang M S, Sherrott M, Lopez J J and Atwater H A 2013 *Nano Lett.* **13** 2541
[7] Guo Q, Li C, Deng B, Yuan S, Guinea F and Xia F 2017 *ACS Photonics* **4** 2989
[8] Hu Y, López-Lorente Á I and Mizaikoff B 2019 *ACS Photonics* **6** 2182
[9] Koppens F H L, Chang D E and De Abajo F J G 2011 *Nano Lett.* **11** 3370
[10] Koppens F H L, Mueller T, Avouris P, Ferrari A C, Vitiello M S and Polini M 2014 *Nat. Nanotechnol.* **9** 780
[11] Yan H, Low T, Zhu W, Wu Y, Freitag M, Li X, Guinea F, Avouris P and Xia F 2013 *Nat. Photon.* **7** 394
[12] Nikitin A Y, Guinea F and Martin-Moreno L 2012 *Appl. Phys. Lett.* **101** 151119
[13] Rodrigo D, Limaj O, Janner D, Etezadi D, De Abajo F J G, Pruneri V and Altug H 2015 *Science* **349** 165
[14] Hu H, Yang X, Guo X, Khaliji K, Biswas S R, De Abajo F J G, Low T, Sun Z and Dai Q 2019 *Nat. Commun.* **10** 1131
[15] Lafkioti M, Krauss B, Lohmann T, Zschieschang U, Klauk H, Klitzing K V and Smet J H 2010 *Nano Lett.* **10** 1149
[16] Chowdhury S F, Sonde S, Rahimi S, Tao L, Banerjee S and Akinwande D 2014 *Appl. Phys. Lett.* **105** 033117
[17] Jo I, Kim Y, Moon J, Park S, Moon J S, Park W B, Lee J S and Hong B H 2015 *Phys. Chem. Chem. Phys.* **17** 29492
[18] Peng S A *et al* 2015 *Carbon N. Y.* **82** 500
[19] Joshi P, Romero H E, Neal A T, Toutam V K and Tadigadapa S A 2010 *J. Phys.: Condens. Matter* **22** 334214
[20] Kim Y J, Lee Y G, Jung U, Lee S, Lee S K and Lee B H 2015 *Nanoscale* **7** 4013
[21] Brenner K and Murali R 2010 *Appl. Phys. Lett.* **96** 063104
[22] Kim Y, Ryu J, Park M, Kim E S, Yoo J M, Park J, Kang J H and Hong B H 2014 *ACS Nano* **8** 868
[23] Farmer D B, Roksana G M, Perebeinos V, Lin Y M, Tuievski G S, Tsang J C and Avouris P 2009 *Nano Lett.* **9** 388
[24] Sun B, Hong W, Thibau E S, Aziz H, Lu Z H and Li Y 2015 *ACS Appl. Mater. Interfaces* **7** 18662
[25] Bareza N J, Gopalan K K, Alani R, Paulillo B and Pruneri V 2020 *ACS Photonics* **7** 879
[26] Rodrigo D, Tittl A, Limaj O, De Abajo F J G, Pruneri V, Altug H, De Abajo F J G, Pruneri V and Altug H 2017 *Light Sci. Appl.* **6** e16277
[27] De Abajo F J G 2014 *ACS Photonics* **1** 133
[28] Hasan D and Lee C 2018 *Adv. Sci.* **5** 1700581
[29] Xu K *et al* 2013 *Nano Lett.* **13** 131
[30] Rabchinskii M K *et al* 2020 *Sci. Rep.* **10** 6902
[31] Walters F *et al* 2020 *Nanomaterials* **10** 1808
[32] Gopalan K K, Paulillo B, Mackenzie D M A, Rodrigo D, Bareza N, Whelan P R, Shivayogimath A and Pruneri V 2018 *Nano Lett.* **18** 5913
[33] Gopalan K K, Rodrigo D, Paulillo B, Soni K K and Pruneri V 2019 *Adv. Opt. Mater.* **7** 1800966
[34] Aksu S, Huang M, Artar A, Yanik A A, Selvarasah S, Dokmeci M R and Altug H 2011 *Adv. Mater.* **23** 4422